

# Evaluation of genetic algorithms for the optimum distribution of viscous dampers in steel frames under strong earthquakes

Xiameng Huang\*

School of Engineering, University of Warwick, Coventry CV4 7AL, U.K.

(Received August 26, 2017, Revised February 9, 2018, Accepted February 10, 2018)

**Abstract.** Supplemental passive control devices are widely considered as an important tool to mitigate the dynamic response of a building under seismic excitation. Nevertheless, a systematic method for strategically placing dampers in the buildings is not prescribed in building codes and guidelines. Many deterministic and stochastic methods have been proposed by previous researchers to investigate the optimum distribution of the viscous dampers in the steel frames. However, the seismic performances of the retrofitted buildings that are under large earthquake intensity levels or near collapse state have not been evaluated by any seismic research. Recent years, an increasing number of studies utilize genetic algorithms (GA) to explore the complex engineering optimization problems. GA interfaced with nonlinear response history (NRH) analysis is considered as one of the most powerful and popular stochastic methods to deal with the nonlinear optimization problem of damper distribution. In this paper, the effectiveness and the efficiency of GA on optimizing damper distribution are first evaluated by strong ground motions associated with the collapse failure. A practical optimization framework using GA and NRH analysis is proposed for optimizing the distribution of the fluid viscous dampers within the moment resisting frames (MRF) regarding the improvements of large drifts under intensive seismic context. Both a 10-storey and a 20-storey building are involved to explore higher mode effect. A far-fault and a near-fault earthquake environment are also considered for the frames under different seismic intensity levels. To evaluate the improvements obtained from the GA optimization regarding the collapse performance of the buildings, Incremental Dynamic Analysis (IDA) is conducted and comparisons are made between the GA damper distribution and stiffness proportional damping distribution on the collapse probability of the retrofitted frames.

**Keywords:** probability of collapse; genetic algorithms; steel MRFs; viscous dampers; interstorey drift

## 1. Introduction

Seismic retrofit with supplemental passive control devices has been demonstrated to be effective for improving the dynamic performance of structures under earthquake excitations. Recent years, change has come to building guidelines that an increasing number of external energy dissipation devices have been used to reduce structural seismic response of taller buildings or to rehabilitate old buildings. The placement of dampers or the distribution of the supplemental damping in the structure may significantly affect the seismic dynamic response and hence affect the overall damping cost. Nevertheless, a systematic method for the optimal damper placement regarding the structural seismic performance objectives does not exist in any of the buildings codes and guidelines (Whittle *et al.* 2012).

The primary problem for the optimization of damper placement is to minimize the seismic response of the buildings by strategically distribute the viscous dampers or the supplemental viscous damping throughout the floors. A large variety and quantity of studies have been performed by previous researchers to investigate the optimal distribution of the dampers in vertical direction. Ashour and

Hanson (1987) suggested that dampers should be placed at the locations where the effective damping ratio of the structural fundamental mode will be maximized. Zhang and Soong (1992) proposed a sequential search method to determine the optimal distribution of viscoelastic dampers in multi-storey structures which is based on the controllability index method (Cheng and Pantelides 1988). Considered its efficiency and effectiveness, the sequential search method was verified by Shukla and Datta (1999) using an elastic single-bay shear frame. Gluck *et al.* (1996) utilized an optimal control method by adapting the linear quadratic regulator to obtain the optimal damper distribution in the elastic shear frame.

Base on a gradient-based approach, Takewaki (1997, 2000) optimized the viscous damper placement in the elastic frame by minimizing the sum of the interstorey drifts in the transfer function. As an evolution of sequential search method, Lopez-Garcia (2001) presented a Simplified Sequential Search Algorithm (SSSA) to find out the optimal solution for the shear frame with linear viscous dampers. Another notable damper optimization method named as Fully-stressed Analysis was proposed by Lavan and Levy (2006, 2009) for both the deterministic analysis and the stochastic analysis. This method utilizes a recurrence relationship to maximize the dampers' effectiveness on the seismic structural performance parameters with a constrained total damping.

Five viscous damper placement methods including the

---

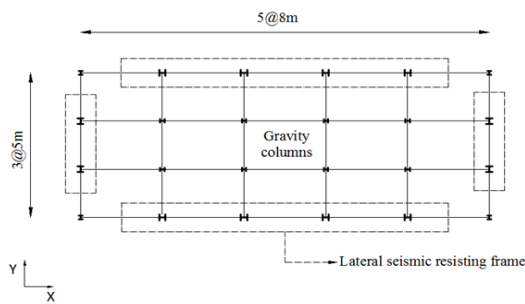
\*Corresponding author, Ph.D. Student  
E-mail: Xiameng.Huang@warwick.ac.uk

uniform damping method, the stiffness proportional damping method, the Takewaki (1997, 2000) method, the SSSA method (Lopez-Garcia 2001) and the Fully-stressed Analysis method (Levy and Lavan 2006, Lavan and Levy 2009) are utilized by Whittle *et al.* (2012) to optimize the dampers of a realistic steel building under the intensity level of Design Basis Earthquake (DBE). Then, the effectiveness and the efficiency of these methods were compared by performing NRH analysis of the building under the intensity levels of Design Basis Earthquake (DBE) and Maximum Considered Earthquake (MCE) respectively. In accordance to Whittle's conclusion, the performance differences between the damper placement strategies are slight under DBE and MCE intensity levels.

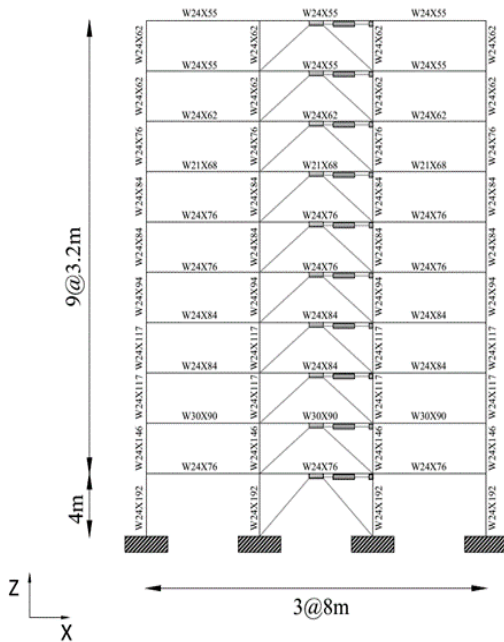
Genetic algorithms (GA), a general search and numerical optimization algorithms inspired by phenomenon adaptation in the natural world, has been widely applied in multiple engineering fields to treat the global optimization problems. Compared to other search algorithms, GA has a stronger capability to explore the potential search space of the optimization problem. GA was noticeably introduced by Singh and Moreschi (2002) to optimize the damper distribution of buildings under stochastic seismic excitation. GA and nonlinear response history (NRH) analysis are

combined by Apostolakis and Dargush (2010) to investigate the optimal seismic design of damper placement with stochastic analysis. Hoffman and Richards (2014) evaluated the efficiency of the GA optimization when used to interface with NRH analysis, based on optimizing the distribution of the buckling restrained braces of a nine-storey building under stochastic design-level ground motions.

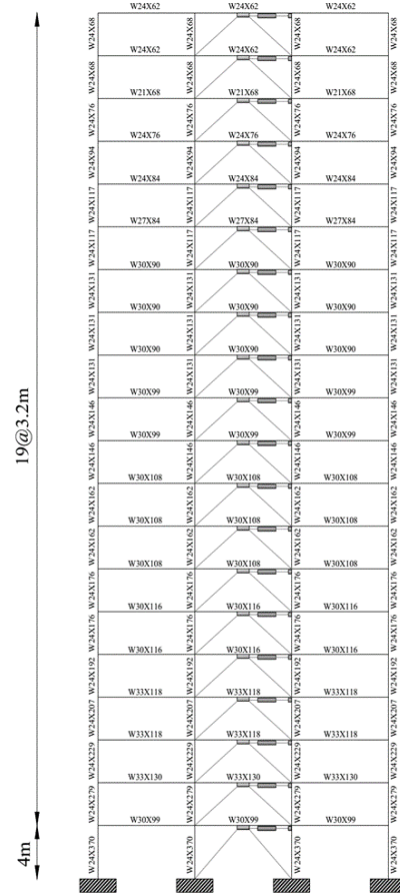
While extensive researches have been conducted to explore the optimization of damper placement throughout the height of the buildings, few of these works assessed the collapse performance of the buildings with the optimized dampers distribution. These works show that in terms of the structural performance parameters under the DBE and MCE, damper optimization throughout the floors does not play a significant role especially the building is with regular distribution of lateral storey stiffness. On the other hand, the combination of GA and NRH is considered as an important and advanced tool to optimally design the buildings while the optimization improvements on the collapse performance haven't been explored by any of the studies. This paper aims to explore whether by optimizing dampers at higher intensity levels, the stochastic optimization with GA and NRH analysis could be beneficial in terms of collapse,



(a) Plan view of the prototype building



(b) Elevation view of the Structure A



(b) Elevation view of the Structure B

Fig. 1 Elevation view of the designed buildings

without compromising the drift behaviour under DBE and MCE. In the present paper, a systematic framework for computationally optimizing the damper distribution regarding the large drift and the collapse of a building is practically established. GA and NRH analysis are combined to form an integrated evolutionary system for the structural optimization. A set of efficient customer setting for the parameters of the GA solver is proposed in this work. Viscous dampers assembled in the moment-resisting steel frames are optimized for a seismic environment under different intensity levels. To evaluate the collapse performance of the optimization results in terms of strong earthquakes, Incremental Dynamic Analyses (IDA) are accordingly implemented and the probabilities of collapse of the optimized damper distributions are compared with those of the stiffness proportional damping distribution. In addition, both far-fault and near-fault earthquakes are considered in this study and MRFs of different stories are involved to explore the influence of higher modes.

## 2. Model definition

Two steel frame structures are considered in the present work. As shown in Fig. 1(a), Structure A is a 10-storey, 5-bay by 3-bay prototype building with two lateral seismic resisting MRFs in the X direction of the perimeter frames. Gravity frames are located in the interior of the building. Structure B is a 20-storey building which has a similar plan view as Structure A. Based on the existing design procedures (EC8 2013, Tzimas *et al.* 2015), the moment-resisting frames in both of the buildings are designed as classical MRFs with linear fluid viscous dampers installed horizontally in the interior bay. Figs. 1(b)-(c) show the elevations of the MRFs with beam and column sizes for Structure A and Structure B respectively. The buildings are designed to be symmetric, hence for two-dimensional analysis in the X direction, a half of the total building mass is assigned to each lateral resisting MRFs and a half of the total plan area is assigned to the 2-D building model as the tributary area. Dampers are connected to the frame through chevron braces which are installed in the interior bays of the MRF.

In accordance to EC8 (2013), the serviceability limits of the peak interstorey drift for both the design cases are selected to be less than 0.75% under the frequently occurred earthquake (FOE). The design basis earthquake (DBE) is defined by the elastic acceleration design spectrum of the EC8 with type B site conditions and 0.35 g peak ground acceleration (PGA). The intensity of the FOE (10% of probability of exceedance in 10 years) is equal to 40% of the intensity of the DBE (10% probability of exceedance in 50 years), and the intensity of the maximum considered earthquake (MCE) (2% probability of exceedance in 50 years) is 50% larger than the intensity of the DBE. The inherent critical damping ratio for the MRFs is assumed to be 3% and a behaviour factor of 6.5 is selected for both the buildings. The estimated peak interstorey drift under DBE ( $IDR_{DBE}$ ) is equal to 1.20% for the frames with dampers and the target peak interstorey drift ( $IDR_t$ ) for the frames

without dampers is estimated to be 1.80%. Hence base on the damping coefficient  $B = IDR_{DBE}/IDR_t = 1.5$ , the total damping ratio is equal to 20% at the first fundamental period ( $T_1 = 2.156$  s for Structure A and  $T_1 = 3.248$  s for Structure B) (Ramirez *et al.* 2002).

## 3. Design supplemental damping

The stiffness proportional damping and the uniform damping methods are conventional and simple damping distribution approaches that are widely applied by previous engineers and researchers (Whittle *et al.* 2012). Stiffness proportional damping system are more effective to reduce the dynamic response of structure as they result in a Rayleigh-type damping matrix which does not lead to complex modes. In the present work, the initial damping coefficients of the dampers in all the stories are designed in accordance to stiffness proportional damping method, from which the damping coefficients of the dampers along the height  $C_j$  is given by

$$C_j = \varepsilon \cdot K_j \quad (1)$$

Where  $\varepsilon$  is a constant that can be derived by the supplemental linear viscous damping  $\beta_v$  and  $K_j$  is the lateral storey stiffness of the steel MRF at storey  $j$ .  $\beta_v$  is obtained simply by subtracting inherent damping from the total damping of the MRFs.  $K_j$  can be determined by utilizing pushover analysis to obtain the ratio between the storey shear force and the interstorey drift displacement at each storey.

Table 1 Designed damping distribution of Structure A and Structure B

Storey	Damping Coefficients (kN · s/m)	
	Structure A	Structure B
1	14842.4	43689.7
2	11363.9	32412.3
3	9682.1	29010.0
4	8557.7	26443.4
5	7596.6	24040.1
6	6900.2	21915.5
7	6211.7	20790.5
8	5423.2	19485.5
9	4772.0	18906.0
10	3971.2	17573.3
11	-	16702.4
12	-	15477.7
13	-	14739.1
14	-	14125.0
15	-	12583.8
16	-	10999.6
17	-	9212.5
18	-	7444.2
19	-	6087.8
20	-	4515.5

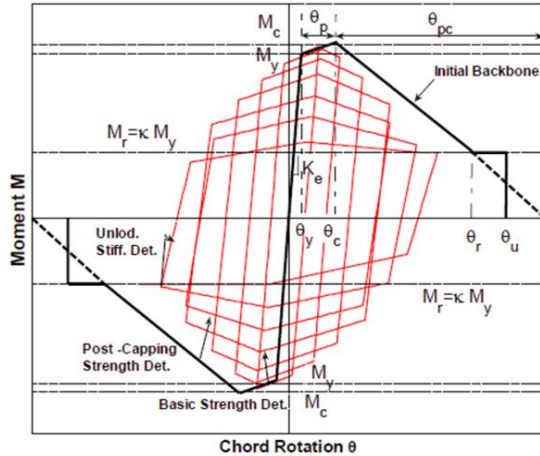


Fig. 2 The illustration of Modified IK Deterioration Model provided by Lignos *et al.* (2010)

Based on the designed supplemental damping distribution of Structure A and Structure B (as shown in Table 1), the corresponding total damping coefficients for the linear viscous dampers of the buildings can be obtained as 79321 kN·s/m and 366153.9 kN·s/m respectively.

## 4. Dynamic analysis

### 4.1 Modeling details

In this study, the OpenSees (2016) program is employed to develop the analytical nonlinear models for the MRFs without brace-dampers and with fluid viscous dampers. Considering the moment-axial force interaction effect, the columns of the MRFs are modeled with the nonlinear force-based fiber elements with distributed plasticity. In accordance to Newell and Uang (2006), heavy columns with webs and flanges of low slenderness, which are similar to the designed columns in this work, do not experience local buckling and cyclic deterioration even under large drifts. Therefore, without considering the cyclic strength and the stiffness deterioration in the column elements, each fiber of the columns is assumed to experience bilinear elastoplastic stress-strain behaviour (refer to 'Steel01 Material' in OpenSees) with strain-hardening ratio of 0.002.

Each beam is modeled as an elastic element with two zero length plastic flexural hinges located at the ends. These zero length plastic hinges are represented by rotational springs that exhibit bilinear hysteretic behaviour of which the rules are described by the Modified Ibarra-Krawinkler Deterioration Model (Lignos *et al.* 2011, Lignos and Krawinkler 2011). The phenomenological model is based on a monotonic backbone curve defined a reference boundary for the hysteretic behaviour of the rotational springs, and a set of rules that describe the hysteretic behaviour between the strength and the deformation bounds of the springs. Specifically, the characteristics of a bilinear hysteretic response are governed by three modes of cyclic deterioration which are the basic yield strength deterioration, the post-capping strength deterioration, and

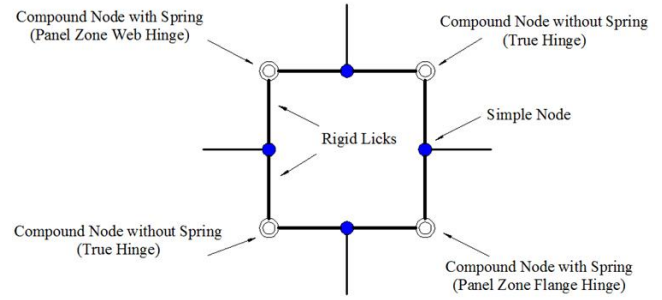


Fig. 3 The illustration of Krawinkler model (panel zone)

the unloading/reloading stiffness deterioration. In terms of these modes, the backbone curve is defined by three strength parameters ( $M_y$  = effective yield strength,  $M_c$  = capping strength, and residual moment  $M_r = \kappa \cdot M_y$ ) and four deformation parameters ( $\theta_y$  = yield rotation,  $\theta_p$  = pre-capping plastic rotation,  $\theta_{pc}$  = post-capping plastic rotation, and  $\theta_u$  = ultimate rotation capacity) respectively. The Modified Ibarra-Krawinkler Deterioration Model and the corresponding deterioration modes are illustrated in Fig. 2. A detailed description for determining the parameters of the modified IK model is presented in the study of Lignos and Krawinkler (2011).

Panel zones of the frames are modelled with the Krawinkler model (Krawinkler 1978) to consider the nonlinear beam-column behaviour. As is illustrated in Fig. 3, this phenomenological model consists of four rigid links connected at the corners by compound nodes. The compound node at upper left corner uses a rotational spring to represent the stiffness and strength of the panel zone web, and the compound node at the lower right corner is set with a rotational spring to represent the column flange bending resistance. The compound nodes at lower left and upper right corner are set to have no stiffness and hence act as true flexural hinges. Twelve nodes in total are used to represent a single Krawinkler model while each corner contains two nodes (one compound node) to constrain x-y and rotational degrees of freedom. Further detailed descriptions for determining the required properties of the panel component refer to (Krawinkler 1978).

Fluid viscous dampers have been demonstrated as an extremely effective device to dissipate seismic energy for structures, since it contains a series of inherent advantages. These advantages include low maintenance required, long-term lifetime, significant self-contained energy dissipation capability and damper forces being out of phase with the elastic forces in the structure (Paola *et al.* 2007). Experimental tests and numerical models to explore the nonlinear behaviour of fluid viscous damper have been developed by Seleemah and Constantinou (1997). Based on these studies, the hysteretic behaviour of fluid viscous dampers can be accurately described by a simple dashpot and the force-velocity relationship is expressed as

$$P(t) = C|\dot{u}(t)|^\alpha \text{sgn}[\dot{u}(t)] \quad (2)$$

Where  $P(t)$  is the damper force;  $C$  is the damping coefficient;  $\dot{u}(t)$  is the velocity across the damper;  $\alpha$  is a velocity exponent which is in the range from 0.3 to 1.0 for

seismic design;  $\text{sgn}[\ ]$  is the signum function. When  $\alpha = 1$ , the damper is a linear viscous damper (Symans *et al.* 2008).

In this study, the linear viscous dampers are modeled as simple linear viscous dashpots. In addition, the damper limit states that could occur with the piston reaching the stroke limit during seismic response are not considered in the analytical model. This is an important assumption for assessing the collapse probability of the frames installed with fluid viscous dampers with limited stroke (Miyamoto *et al.* 2010). It is essential be noted that typical stroke limit of the dampers in the market is around  $\pm 100$  mm and strokes of fluid viscous dampers can be extensible up to  $\pm 900$  mm upon request (Taylor Devices 2017). With an extended stroke limit, the dampers in the MRFs presented in this study do not reach the limit states even when the frame reaches the collapse state and undergoes a significant interstorey drift. The chevron braces are assumed to be strong enough to resist the maximum damper forces and the brace buckling due to excessive damper force are therefore not considered in this model. In this case, the diagonal braces are modeled using elastic truss elements (OpenSees 2016).

With the consideration of material and geometric nonlinearity, a 'lean-on' column is arranged to model the gravity frame and to simulate the  $P$ - $\Delta$  effects that results from the vertical loads imposed on the tributary area of frame. The 'lean-on' column is modeled with elastic beam column elements with assigned floor mass at each floor level. To model the diaphragm action, the horizontal displacement of the nodes along the length of the beams at each floor level are constrained to the node in the 'lean-on' column at the corresponding floor level, using truss elements (OpenSees 2016).

Rayleigh damping is modelled with 3% damping at first two modes of the vibration corresponding to the 3% inherent critical damping of the frames. The Newmark method with constant acceleration and the Newton-Raphson algorithm with tangent stiffness are used to solve the nonlinear dynamic equations while evaluating the seismic response of the frames.

#### 4.2 Ground motions

To explore the effectiveness of the GA optimization in terms of collapse on different seismic characteristics, both far-fault and near-fault ground motions are considered in this study. A set of 44 far-fault recorded ground motions selected by ATC-63 project (FEMA 2008) are used for conducting the NHR analysis. A set of 20 near-fault ground motions are developed based on the set of 91 pulse-like ground motions selected by Baker (2007) from the PEER NGA. This set of near fault quakes are selected based on the critical region of the ratio between the pulse period and the fundamental period  $T_p/T_1 \geq 2$  which was found by Champion (2012). In accordance to Champion's study, the collapse capacity of the near fault earthquakes decreases significantly within this specific region. It should be noted that the fundamental period of the Structure A is used to develop the near-fault ground motions in this study. The set of 20 near-fault ground motions are selected in series within

the region  $2.00 \leq T_p/T_1 \leq 3.50$  ( $4.50 \text{ s} \leq T_p \leq 7.50 \text{ s}$  for  $T_1 = 2.156 \text{ s}$ ). This set of near-fault ground motions are also applied on Structure B to perform optimization. In this case, the ratio between the pulse period and the fundamental period of Structure B is given as  $1.38 \leq T_p/T_1 \leq 2.31$  for  $T_1 = 3.248 \text{ s}$ . The mean PGA and the mean duration of the 44 far-fault ground motions suite are  $0.39 \text{ g}$  and  $71.21 \text{ s}$ . For the 20 near-fault ground motions suite, the mean PGV and the mean duration are  $64.71 \text{ cm/s}$  and  $79.21 \text{ s}$ . Detailed information of the 44 far-fault ground motions and the 91 near-fault ground motions, including the explanations for the motion selections in terms of collapse evaluation, refer to ATC-63 project (FEMA 2008) and Baker (2007) respectively.

#### 4.3 Evaluation for probability of collapse

Incremental Dynamic Analysis (IDA) (Vamvatsikos and Cornell 2002) is used to evaluate the collapse probability of the structures initially designed with dampers from stiffness proportional damping method. According to IDA, each ground motion record is increasingly scaled to preform NRH until the collapse of the structure is caused, in order to estimate the relationships between intensity measure (IM) and engineering demand parameter (EDP). In this study, the spectral acceleration at the fundamental period of the structure  $S_a(T_1)$  is selected as IM and the maximum interstorey peak drift  $\theta_{\max}$  is used as EDP to monitor the dynamic instability. Both the sets of the 44 far-fault ground motion records and the 20 near-fault ground motion records are involved to preform IDA to obtain the collapse probability of Structure A and Structure B.  $S_a(T_1)$  is scaled up in an increment of  $0.005 \text{ g}$  from  $0.005 \text{ g}$  until the frame model start to collapse due to the seismic lateral force. The monitoring boundary for  $\theta_{\max}$  is set at 15%.

Base on the results of the  $S_a(T_1)$  at the collapse intensity, the probability fragility curves for all cases are accordingly constructed by fitting a lognormal cumulative distribution function to provide a continuous of evaluation of the collapse probability as a function of  $S_a(T_1)$ . While constructing the fragility curves, the spectral acceleration for 3% effective damping  $S_a(T_1)$  is multiplied by the damping coefficient ( $B = 1.154$ ) to represent the spectral acceleration for 5% effective damping  $S_a(T_1, 5\%)$ . Then  $S_a(T_1, 5\%)$  is normalized by the MCE spectral acceleration at the fundamental period of the structure  $S_{a,MCE}(T_1)$ , to straightforwardly represent the collapse margin ratio (CMR). According to the ATC-63 project, CMR is a cardinal Index to for collapse assessment and seismic design criteria. It is defined as the median intensity which would result in collapse in 50% of the structures subjected to each considered ground motion (FEMA 2008). This ratio is normally obtained by normalizing the median 5%-damped spectral acceleration at fundamental period  $\hat{S}_{a,COL}(T_1)$  by the 5%-damped spectral acceleration of the MCE at fundamental period  $S_{a,MCE}(T_1)$ .

$$CMR = \frac{\hat{S}_{a,COL}(T_1)}{S_{a,MCE}(T_1)} \quad (3)$$

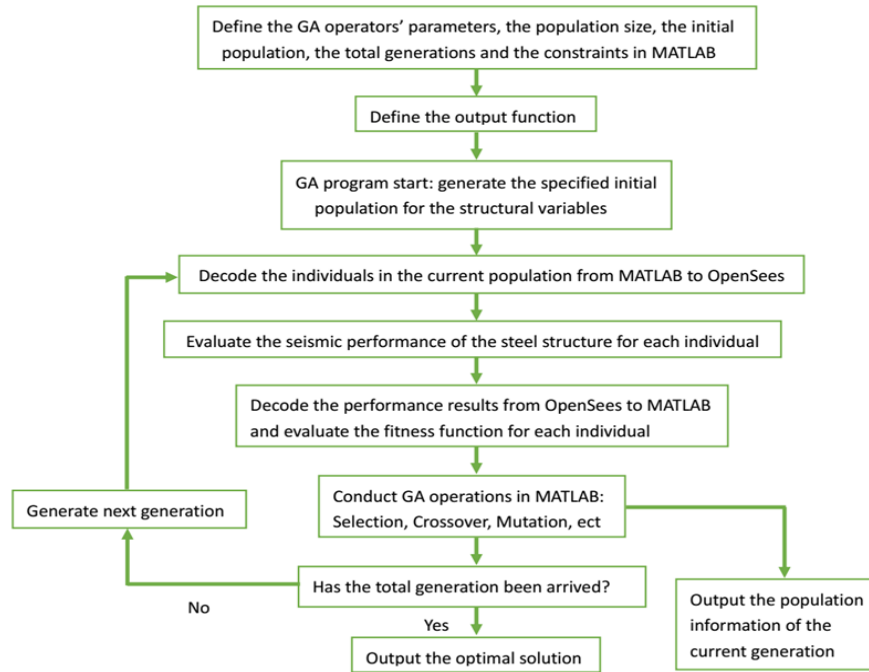


Fig. 4 The GA-NRH optimization framework

## 5. Computational optimization

### 5.1 Optimization framework

Genetic algorithms (GAs) are general search and numerical optimization algorithms inspired by the phenomenon adaptation in the natural world. More specifically, the GA approach imitates the evolution of species by both natural selection and natural genetics. After it was first introduced by Holland in 1960s (Holland 1992), this approach has been gaining a growing following in the physical, computer systems, social science and engineering.

GAs are initialized with a population of guesses within the search space instead of starting from a single guess. Typically, an initial population is modeled as a binary encoding or a string associated with true variables, which has a similar structure with a chromosome. Selection, crossover and mutation are chosen as the three main operators to direct the population by analogy with the natural world. Over a series of generations processed by these three operators, the population are directed towards convergence at the global optimum (Coley 1999).

For a practical engineering application, this work presents a structural optimization framework which is based on utilizing the genetic algorithms from the Global Optimization Toolbox of MATLAB (MATLAB 2014) and the dynamic time history analysis from the OpenSees (OpenSees 2016). Seismic design is considered as a complex adaptive process and the numerical dynamic time history analysis is embodied into the computational framework of the GA in MATLAB to evaluate the seismic performance of the retrofitted structures.

The entire process is divided into three main steps. For the first step, a finite element model in term of the specific

optimization case is built up with the help of OpenSees to provide the seismic Nonlinear Response History (NRH) analysis of the steel frame. For the second step, the GA framework including fitness function, constraint functions, output functions and the GA solver commands, is established in the MATLAB files. Finally, the results in the outputs documents obtained from NRH analysis are assigned to the variables of the fitness function in MATLAB and hence the adaptive evolutionary loops are formed.

After constructing the GA-NRH loops, the parameters for the GA operators are defined based on the specification of the MATLAB Documentation and the general principle of the GA global search, in order to achieve the relative global optimum convergence. The detailed procedures of the theoretical optimization framework are shown in Fig. 4.

### 5.2 Optimization problem

In order to quantify the performance of each retrofitted structure, a fitness function has to be defined in terms of the seismic performance index of the structure. For the present work, the maximum interstorey peak drift, which is one of the most cardinal performance index for satisfying the serviceability and the collapse limitations, is selected to establish the fitness function (Takewaki 1997, Lavan and Levy 2009). The fitness function expected to be minimized is defined as

$$Fitness = \theta_{\max} \quad (4)$$

While

$$\theta_{\max} = \max \left( \frac{|d_j(t) - d_{j-1}(t)|}{h_j} \right) \quad (5)$$

For

$$0 \leq t \leq T_{total} \text{ and } j = 1, \dots, N_{total}$$

where  $d_j(t)$  is the displacement relative to the ground at time  $t$  at  $j$  storey of the frame,  $h_j$  is the height of storey  $j$ ,  $T_{total}$  is the total duration of the earthquake excitation and  $N_{total}$  is the total storey number of the frame.

Hence the basic optimization problem becomes to minimize the maximum interstorey peak drift of the seismic resisting frames by adaptively distribute the damping coefficients of the viscous dampers in all the stories. While conducting the optimizations, the supplemental total damping coefficients for the retrofitted frame are constrained by the same total damping coefficients obtained from the stiffness proportional damping design. The theoretical constrained function for the GA is defined as

$$C_{total} = \sum_{j=1}^{N_{total}} C_j \quad (6)$$

### 5.3 Intensity levels and ground motions considered

As is mentioned in the previous section, four optimization cases are considered as Structure A under 44 far-fault ground motions (Case 1); Structure A under 20 near-fault ground motions (Case 2); Structure B under 44 far-fault ground motions (Case 3); and Structure B under 20 near-fault ground motions (Case 4). For each optimization case, a targeted ground motion record is selected to conduct single objective optimization within the GA-NRH framework. As the aim of this work is to improve the probability of collapse in terms of a given seismic environment, the selected targeted ground motion, to some extent, should be able to represent the seismic characteristic of this ground motions environment utilized to perform collapse simulation. In accordance to the ATC-63 project (FEMA 2008), the median drift or the average drift for a set of ground motions can be treated as the criteria for determining column axial failure that caused non-simulated collapse. Therefore, the single targeted ground motion used to optimize collapse can be determined by comparing the drift level caused by each ground motion with the median drift level. If a drift level caused by a ground motion is more similar to the median drift level than the drift levels caused by other ground motions, this ground motion could be used to represent the set of ground motions in terms of structural performance. However, the structures' sensitivity to the performance level could vary with the magnitude of earthquake. According to the previous researchers, the optimized damping distribution under lower intensity levels (e.g. DBE and MCE) are normally not workable for improving the structural performance associated with higher intensity levels (Whittle *et al.* 2012). The present study therefore uses various intensity levels especially higher intensity levels to explore the seismic optimization efficiency in terms of the collapse performance. Hence, four representative ground motion records are selected for the four optimization cases in accordance to the selection criteria mentioned above, based on the IDA results of the initial damper design.

For the Case 1 optimization, the intensities used to conduct the optimization are conservatively selected at the DBE, 3DBE (i.e., 3 times of DBE) and 4MCE (i.e., 4 times of MCE) which is the medium seismic intensities of the fragility curves. The intensity levels applied for Case 2, Case 3 and Case 4 optimization are set at MCE&2MCE, 5MCE and 5MCE respectively, which are closed to the medium seismic intensities of the fragility curves.

With the specified objective intensity levels, the target ground motion for an optimization case could be located, by selecting a representative ground motion from the corresponding ground motion groups in terms of the maximum peak interstorey drift  $\theta_{max}$  of the building under the objective seismic intensity. Based on the IDA results, the reference values of the  $\theta_{max}$  for determining the representative ground motions are simply obtained by calculating the median values and the average values of the  $\theta_{max}$  of the all the ground motions which maintain the building to be stable rather than collapsed under the associated objective intensities. For the case more than 20 ground motions 'survive' under the objective intensity in a ground motion group, the median value of the  $\theta_{max}$  for the 'survived' ground motions is used to dominate the selection of the representative ground motion, which means that the  $\theta_{max}$  from the representative ground motion should be more closed to the median value rather than the average value of the 'survived' ground motions. For the case less than 20 ground motions 'survive' under the objective intensity, the average value of the  $\theta_{max}$  for the 'survived' ground motions is utilized to dominate the selection of the representative ground motion due to the consideration of mathematic discreteness. Accordingly, the representative ground motions for these four optimization cases are respectively determined as the No.31 earthquake of the 44 far-fault ground motions group (FE31) for Case 1 (DBE and 3DBE) optimization, the No.27 earthquake of the 44 far-fault ground motions group (FE27) for Case 1 (4MCE) optimization, the No.4 earthquake of the 20 near-fault ground motions group (NE4) for Case 2 (MCE) optimization, the No.6 earthquake of the 20 near-fault ground motions group (NE6) for Case 2 (2MCE) optimization, the No.29 earthquake of the 44 far-fault ground motions group (FE29) for Case 3 (5MCE) optimization and the No.11 earthquake of the 20 near-fault ground motions group (NE11) for Case 4 (5MCE) optimization.

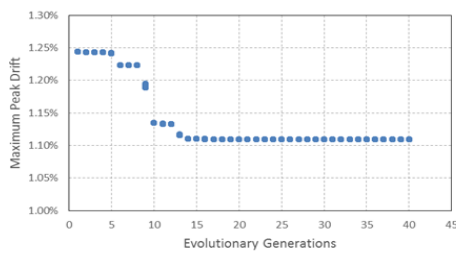
### 5.4 GA optimization parameters

The basic evolutionary operators for the GA is generally known as selection, crossover and mutation that are utilized to promote the evolution of the population by constantly exploring the search space and maintaining the characteristic diversity of the population. Different kind of engineering optimization problems could have different GA solutions with various combinations of the operator parameters. Furthermore, the computational efficiency and the optimization accuracy for a single optimization problem are significantly affected by the determination for the parameters. Since the algorithms structure and the coding

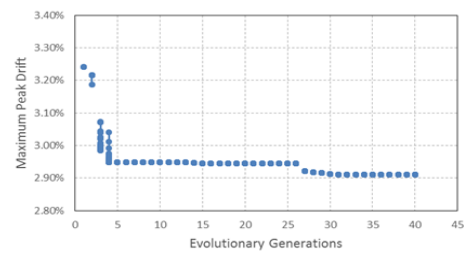
Table 2 The option parameters of the GA solver in MATLAB

Option Parameters	Value
'InitialPopulation'	damp0
'PopulationSize'	50
'Generations'	40
'SelectionFcn'	@selectionroulette
'CreationFcn'	@gacreationlinearfeasible
'CrossoverFcn'	{@crossoverintermediate, 30}
'CrossoverFraction'	0.5
'MutationFcn'	@mutationadapftfeasible
'MigrationInterval'	100
'MigrationFraction'	0.2
'EliteCount'	3
'TolCon'	1e-1000
'TolFun'	1e-1000

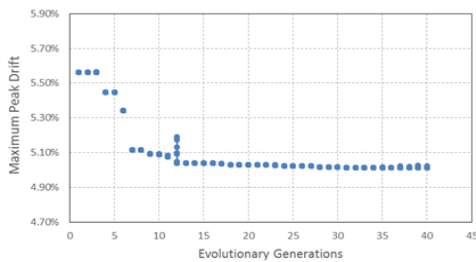
sophistication of the GA tools vary greatly, the distributions for the operators' parameters also have various preferences. MATLAB official guiding documentations clearly provide the recommended parameters' regions in terms of the constrained optimization problems with GA, which is corresponding to the optimization problems in the present work. Based on these recommendations, a set of highly effective parameters combinations is found by try-and-error and monitoring the intermediate variation of the evolutionary population with the help of output function. With this parameter combination, the optimization solutions are able to converge to relatively global optimum instead of unaccepted local optimum before 30 generations. The parameters of the GA solver, which is based on the function 'gaoptimset', are defined as shown in Table 2.



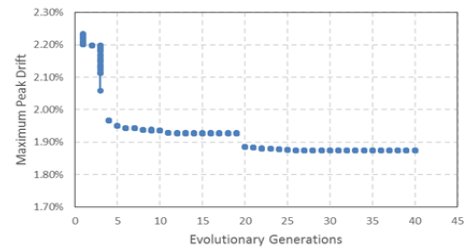
(a) The evolutionary fitness of GA(DBE) in Case 1 optimization



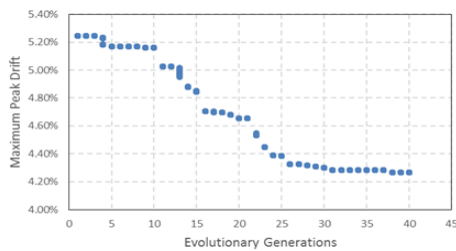
(b) The evolutionary fitness of GA(3DBE) in Case 1 optimization



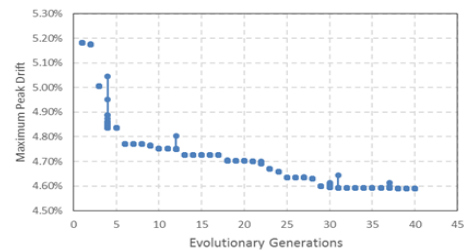
(c) The evolutionary fitness of GA(4MCE) in Case 1 optimization



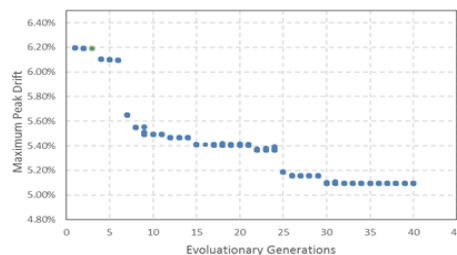
(d) The evolutionary fitness of GA(MCE) in Case 2 optimization



(e) The evolutionary fitness of GA(2MCE) in Case 2 optimization



(f) The evolutionary fitness of GA(5MCE) in Case 3 optimization



(g) The evolutionary fitness of GA(5MCE) in Case 4 optimization

Fig. 5 The evolutionary processes of the optimizations

It is important to note that the initial populations for the GA solver is defined as ‘damp0’ which is corresponding to the initial designed stiffness proportional damping distributions of the frames. The size of the evolutionary populations is set as 50 and it is assumed that it takes 40 generations for the initial population to evolve into relatively optimal population. Roulette selection is used as the selection operator and elite number is set at 3 for each generation. As is shown in Table 2, other option parameters are defined in accordance to the specific recommendation in MATLAB manual document in terms of constrained optimization with GA.

## 6. Results and discussion

### 6.1 Optimization for the representative earthquakes

Based on the established computational framework of GA optimization and the assigned parameters of operators, the Ga analysis for each optimization case is run by 40 generations towards the relatively minimized peak drifts of all the storeys. The intermediate computational data of the GA solver are output by adding an additional output function in the MATLAB files in order to monitoring the convergence process of the GA population. For Case 1 optimization, the evolutionary process of the fitness of the GA population individuals are shown in Figs. 5(a)-(c). Figs. 5(d)-(e) illustrate the fitness evolution of Case 2 optimization while Figs. 5(f)-(g) represent the convergence process of Case 3 and Case 4 optimization respectively. All these diagrams indicate that the GA analyses achieve high performance in terms of the population convergence and the global optimum. The maximum peak interstorey drifts for both structures are reduced by around 10% under the far-fault earthquakes and the peak drifts under near-fault earthquakes are dramatically improved by approximately 18%. The damping distributions obtained from the GA optimizations for all the study schemes are shown in Figs. 6(a)-(d). As can be seen from the figures, given that the GA solver initiates the search from the stiffness proportional damping distribution, the damping values for most of the stories show significant differences between the converged optimal damping distribution and the original distribution. This phenomenon indicates that the GA solver leads the populations to the global optimum by exploring extremely deep search space.

Tables 3-8 present the specific values of the maximum interstorey peak drift ratio (IDR) of the representative earthquakes used to conduct the optimization. In these tables, comparisons are made between the stiffness proportional damping distribution and the distribution obtained from GA schemes under various intensity levels. It is observed that the improvement for the peak drifts in terms of the GA schemes under the intensity levels of the optimizations are significant. However, for other considered intensity levels which are not utilized to conduct the optimization, the peak drifts of the structures are not improved sharply and even increased slightly in some cases.

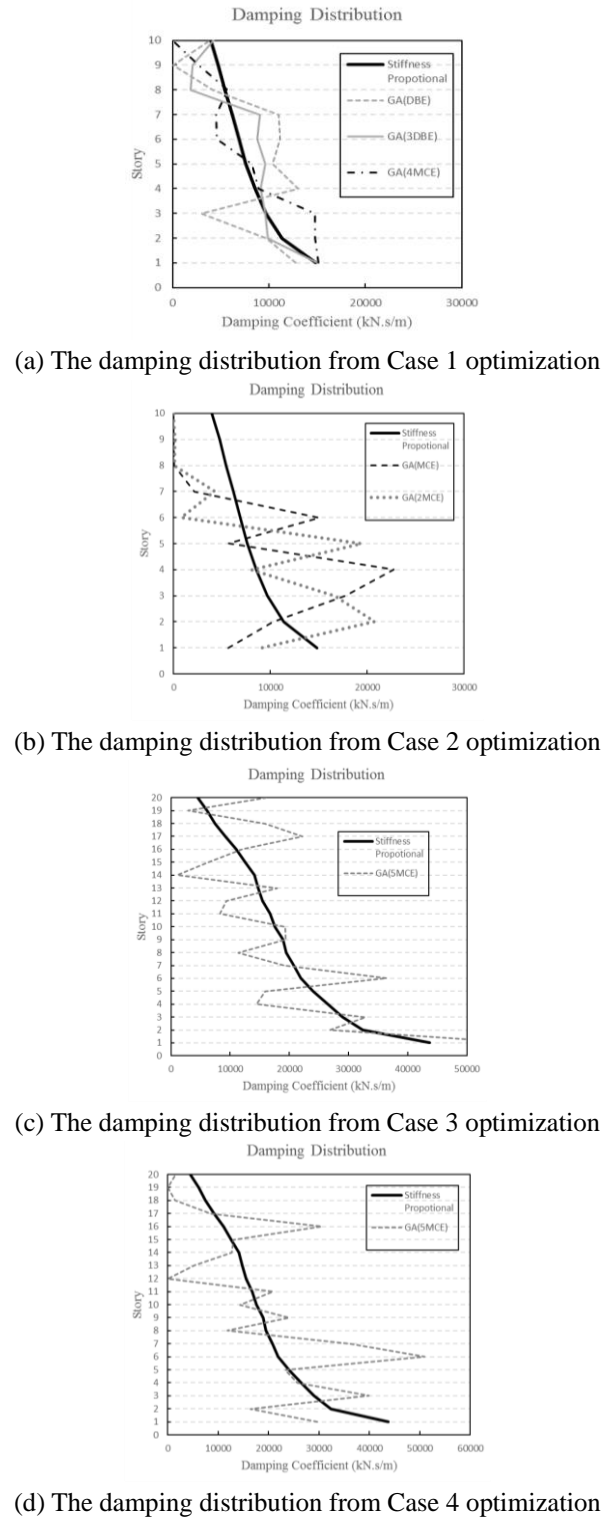


Fig. 6 The damping distributions obtained from the optimizations

Table 3 Peak drifts of the representative quake (Case1-FE31) for GA(DBE) and GA(3DBE) optimization in terms of different damping distributions

Building	IDR <sub>DBE</sub>	IDR <sub>3DBE</sub>
Stiffness	1.24%	3.24%
GA(DBE)	1.11%	3.23%
GA(3DBE)	1.18%	2.91%

Table 4 Peak drift of the representative quake (Case 1-FE27) for GA(4MCE) optimization in terms of different damping distributions

Building	IDR <sub>DBE</sub>	IDR <sub>MCE</sub>	IDR <sub>2MCE</sub>	IDR <sub>3MCE</sub>	IDR <sub>4MCE</sub>
Stiffness	0.68%	1.06%	2.23%	3.56%	5.57%
GA(4MCE)	0.73%	1.08%	2.29%	3.61%	5.01%

Table 5 Peak drift of the representative quake (Case 2-NE4) for GA(MCE) optimization in terms of different damping distributions

Building	IDR <sub>DBE</sub>	IDR <sub>MCE</sub>	IDR <sub>1.5MCE</sub>	IDR <sub>2MCE</sub>
Stiffness	1.31%	2.28%	4.41%	8.53%
GA(MCE)	1.18%	1.87%	4.23%	7.98%

Table 6 Peak drift of the representative quake (Case 2-NE6) for GA(2MCE) optimization in terms of different damping distributions

Building	IDR <sub>DBE</sub>	IDR <sub>MCE</sub>	IDR <sub>1.5MCE</sub>	IDR <sub>2MCE</sub>
Stiffness	1.20%	2.16%	3.53%	5.25%
GA(2MCE)	1.17%	1.96%	3.10%	4.26%

Table 7 Peak drift of the representative quake (Case 3-FE29) for GA(5MCE) optimization in terms of different damping distributions

Building	IDR <sub>DBE</sub>	IDR <sub>MCE</sub>	IDR <sub>2MCE</sub>	IDR <sub>3MCE</sub>	IDR <sub>4MCE</sub>	IDR <sub>5MCE</sub>
Stiffness	0.76%	1.13%	1.95%	2.96%	3.78%	5.18%
GA(5MCE)	0.82%	1.23%	2.16%	3.27%	4.05%	4.59%

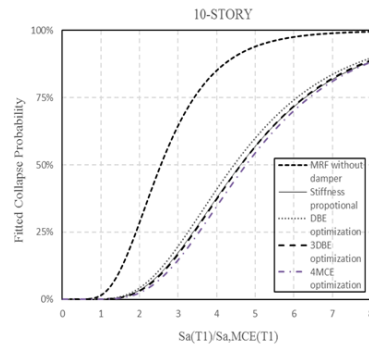
Table 8 Peak drift of the representative quake (Case 4-NE11) for GA(5MCE) optimization in terms of different damping distributions

Building	IDR <sub>DBE</sub>	IDR <sub>MCE</sub>	IDR <sub>2MCE</sub>	IDR <sub>3MCE</sub>	IDR <sub>4MCE</sub>	IDR <sub>5MCE</sub>
Stiffness	0.54%	0.82%	1.70%	2.80%	4.46%	6.20%
GA(5MCE)	0.54%	0.80%	1.57%	2.42%	3.82%	5.09%

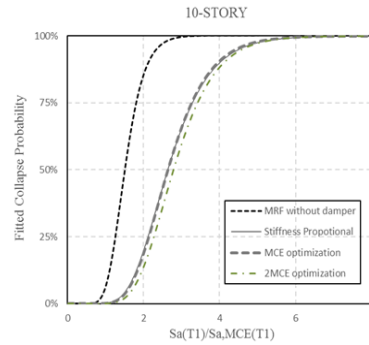
### 6.2 Collapse simulation

To evaluate the sideways collapse mechanism influenced by the optimized damping distribution, incremental dynamic analyses (IDA) are performed for all optimization cases including the corresponding steel MRFs without damper installation. The fitted fragility curve of collapse probability for all the damping distribution schemes of the four optimization cases are shown in Figs. 7(a)-(d). The fragility curves of the associated bare steel MRFs are also plotted in Figs. 7(a)-(d) for comparison. Based on the calculation results from IDA, the median or the average values for the maximum interstorey drift ratio (IDR) of the 44 far-fault earthquakes and the 20 near-fault earthquakes in terms of lower seismic intensities are given in Tables 9-12. The collapse margin ratios (CMR) for the considered steel MRFs as well as the MRF without damper are also presented in the tables.

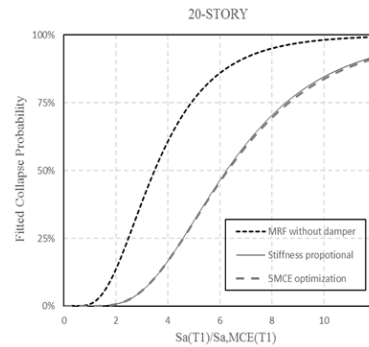
As shown in Fig. 7(a), the fragility curve for the DBE optimization damping distribution of Case 1 (10-storey building under 44 far-fault earthquakes) is slightly shifted to



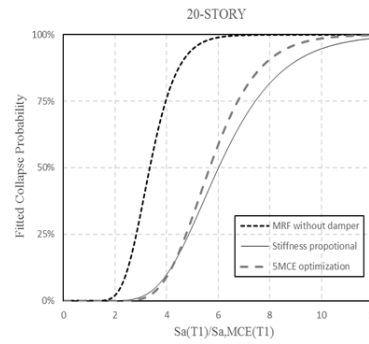
(a) Fitted probability of collapse for Case 1 optimization



(b) Fitted probability of collapse for Case 2 optimization



(c) Fitted probability of collapse for Case 3 optimization



(d) Fitted probability of collapse for Case 4 optimization

Fig. 7 The probability of collapse for the optimizations

left with respect to that for the stiffness proportional damping distribution, indicating that the optimization under DBE intensity levels even results in marginally greater likelihood of building collapse under most of the intensity levels. While the fragility curve for the 3DBE optimization distribution coincides exactly with that for the stiffness proportional distribution, the fitted collapse probability for

Table 9 Median peak drifts of 44 far-fault quakes in terms of different damping distributions (Case 1)

Building	CMR	IDR <sub>DBE</sub>	IDR <sub>MCE</sub>	IDR <sub>1.5MCE</sub>
Bare MRF	2.55	2.02%	2.60%	-
Stiffness	4.62	0.96%	1.49%	2.37%
GA (DBE)	4.45	0.95%	1.52%	2.40%
GA (3DBE)	4.63	0.97%	1.50%	2.30%
GA (4MCE)	4.77	0.98%	1.50%	2.36%

Table 10 Average peak drifts of 20 near-fault quakes in terms of different damping distributions (Case 2)

Building	CMR	IDR <sub>DBE</sub>	IDR <sub>MCE</sub>
Bare MRF	1.50	2.22%	5.27%
Stiffness	2.63	1.26%	2.38%
GA (MCE)	2.64	1.21%	2.31%
GA (2MCE)	2.78	1.22%	2.19%

Table 11 Median peak drifts of 44 far-field quakes in terms of different damping distributions (Case 3)

Building	CMR	IDR <sub>DBE</sub>	IDR <sub>MCE</sub>	IDR <sub>1.5MCE</sub>
Bare MRF	3.49	1.89%	2.25%	-
Stiffness	6.26	0.62%	0.91%	1.36%
GA (5MCE)	6.29	0.69%	1.00%	1.52%

Table 12 Average peak drifts of 20 near-fault quakes in terms of different damping distributions (Case 4)

Building	CMR	IDR <sub>DBE</sub>	IDR <sub>MCE</sub>	IDR <sub>1.5MCE</sub>
Bare MRF	3.35	1.03%	1.58%	-
Stiffness	6.02	0.55%	0.81%	1.43%
GA (5MCE)	5.67	0.56%	0.84%	1.45%

4MCE optimization are somewhat improved at a given intensity level. The comparison between the CMR values shown in Table 9 straightforwardly represents the variation for the overall collapse probability caused by the optimizations. The IDR presented in Table 9 indicates that the seismic performances of the frame under 44 far-fault earthquakes for all considered damping distributions are similar at the lower intensity levels (less than 2MCE) where none of the earthquake results in collapse failure. Fig. 7(b) shows that the probability fragility curve for the MCE optimization damping distribution of Case 2 (10-storey building under 20 near-fault earthquakes) are similar to that for the stiffness proportional damping distribution. However, the fragility curve for the 2MCE optimization strategy is slightly shifted to right compared to that for stiffness proportional strategy. It is observed from Table 10 that both the CMR and the averaged IDR values are slightly improved by the 2MCE optimization.

Fig. 7(c) shows that the collapse fragility curve for the 5MCE optimization damping distribution of Case 3 (20-storey building under 44 far-fault earthquakes) approximately coincide with the one for the stiffness proportional damping distribution. Additionally, Table 11 indicated that the median IDR of the 5MCE optimization are to some extent amplified under the intensity levels of

Table 13 Collapse intensities and the DBE interstorey drift ratios for the representative earthquakes

Building	Damping Distribution	Earthquake	IDR <sub>DBE</sub>	Collapse Intensity (m/s <sup>2</sup> )
10-storey	GA(DBE)	FE31	1.11%	2.04
	GA(3DBE)	FE31	1.18%	1.945
	Stiffness proportional	FE31	1.24%	1.94
	GA(4MCE)	FE27	0.73%	2.32
	Stiffness proportional	FE27	0.68%	2.125
	GA(MCE)	NE4	1.17%	0.84
	Stiffness proportional	NE4	1.30%	0.815
	GA(2MCE)	NE6	1.17%	1.195
	Stiffness proportional	NE6	1.19%	1.13
	20-storey	GA(5MCE)	NE29	0.82%
Stiffness proportional		NE29	0.76%	1.02
GA(5MCE)		NE11	0.54%	1.205
Stiffness proportional		NE11	0.54%	1.235

DBE, MCE and 1.5MCE. As can be seen from Fig. 7(d) that the fragility curve for the 5MCE optimization of Case 4 (20-storey building under 20 near-fault earthquakes) is dramatically shifted to left at higher intensity levels, indicating that the damping optimization strategy of Case 4 lead to greater likelihood of building collapse under a given high intensity level.

To further investigate the collapse performance of the GA optimization damping distribution, the boundary intensities of the collapse failure for the representative earthquakes are presented in Table 13 in terms of the considered GA damping distribution. As can be seen, the collapse intensity for the 10-storey building is improved by around 9% under the far-fault representative earthquake (FE27-4MCE) and up to 6% under the near-fault representative earthquake (NE6-2MCE), respected to stiffness proportional distribution. For the GA optimizations under the representative earthquakes at the lower intensity levels (FE31-DBE, FE31-3DBE and NE4-MCE), the improvements for the collapse intensities of the 10-storey building are significantly less than that under the higher intensity levels (FE27-4MCE and NE6-2MCE). In terms of the 20-storey building under the representative earthquakes, the collapse intensity is increased by solely 1% with the FE29-5MCE optimization and even reduced by 2% with the NE11-5MCE optimization. It is observed that the performance of the optimized frames under the single representative earthquakes basically coincide with that under the 44 far-fault earthquakes and 20 near-fault earthquakes, indicating that the utilized representative quakes are able to represent the seismic characteristics of the earthquakes groups.

To summarize, the GA optimization efficiency for a single representative near-fault earthquake could be normally larger than that for a single representative far-fault earthquake. The GA optimization at an intensity level for an

earthquake or an earthquake group is more effective to the seismic performance around the optimized intensity level than other intensity levels. Similarly, the GA optimization efficiency regarding the collapse failure for both a single earthquake and an earthquake group are considered to be more significant at a relatively high optimized intensity level other than a low optimized intensity level. On the other hand, the GA optimization in terms of collapse failure under the 44 far-fault and the 22 near-fault earthquakes context are less effective to the 20-storey building rather than the 10-storey building. That could be explained by the amplified effect to the problem search space caused by the increase of the building vibration mode. Although the improvement regarding seismic performance contributed by the GA distribution for a single representative earthquake at a targeted intensity level is significant, both the CMR value to an earthquake group and the ultimate collapse intensity level to a single representative earthquake are not dramatically improved.

## 7. Conclusions

Optimization of damper placement for the building under seismic loading is an important topic in structural engineering. The general optimization problem for damper placement is to minimize the seismic response of the building by optimally distribute the viscous dampers throughout the height of the building. Multiple stochastic studies are carried out by the previous researchers to optimize the damper distribution. Moreover, most of the previous studies solely optimize the buildings with a single earthquake record under a design-level earthquake which would not lead to the collapse failure of the building. None of the studies has considered the effectiveness of the damper distribution strategies in terms of the probability of collapse under a series of earthquakes context (e.g., the 44 ground motion records selected by FEMA).

This study utilizes GA interfaced with the NHR analysis to explore the feasibility of the stochastic optimization for the damper distribution under strong earthquakes. Beyond example in this field, collapse simulation and objective optimization regarding large interstorey drifts are introduced to the GA optimization. A 10-storey MRF and a 20-storey MRF are both included to investigate the reliability and the efficiency of the optimization framework. In order to explore the general collapse capacity of the building, the 44 far-fault earthquakes group and the 20 near-fault earthquake group are both included to perform Incremental Dynamic Analysis. Corresponding representative earthquakes records are selected to conduct the optimization based on the initial IDA results. In order to investigate the damper retrofitted efficiency with respect to collapse, multiple seismic intensity levels are involved to minimize the interstorey peak drift with a fixed total supplemental damping.

The results of this work show that the efficiency of the GA optimization is acceptable, while considering a single earthquake at a certain intensity level. However, a baseline study implies that the stochastic GA optimization at a

certain intensity level cannot efficiently improve the general collapse probability of a building, especially when the optimization is under a design-based intensity level. This finding is in line with a previous one from Whittle *et al.* (2012), while this work expands the conclusion of Whittle *et al.* from design level earthquakes to earthquakes of larger magnitude triggering collapse. Furthermore, since GA has been considered as one of the most powerful search algorithms, other stochastic search methods are not expected to obtain a better damper distribution than GA. Hence, this study initially reveals that the stochastic analyses might not be efficient to optimize the damper distribution of the buildings with respect to collapse performance.

Considering the seismic characteristics of the natural earthquakes vary greatly, the stiffness proportional damping distribution of dampers throughout the floors is more stable to reduce the structural response caused by the earthquakes of different magnitude and frequency. For common regular designed buildings, general stochastic optimization of damping distribution without considering collapse might not be practically applied to building constructions, since the collapse performance might not be as acceptable as that from the stiffness proportional damping distribution. It is also important to note that the added damping distribution of taller buildings might be less feasible to optimize in terms of collapse performance, as the complex vibration modes could dramatically expand the problem search space and enlarge the discreteness of the structural response. In contrast, stiffness proportional damping distribution, which result in a Rayleigh-type damping matrix and hence does not lead to complex modes, might be more suitable for the design of taller buildings.

## Acknowledgments

The author thanks Professor Theodore Karavasilis of the Faculty of Engineering and the Environment at the University of Southampton for his help in carrying out the computational analyses.

## References

- Apostolakis, G. and Dargush, G.F. (2010), "Optimal seismic design of moment-resisting steel frames with hysteretic passive devices", *Earthq. Eng. Struct. Dyn.*, **39**, 355-376.
- Ashour, S.A. and Hanson, R.D. (1987), "Elastic seismic response of buildings with supplemental damping", Report No. UMCE 87-01, Department of Civil Engineering, University of Michigan, Ann Arbor, MI, USA.
- Baker, J.W. (2007), "Quantitative classification of near-fault ground motions using wavelet analysis", *Bull. Seismol. Soc. Am.*, **97**(5), 1486-1501.
- Champion, C. and Liel, A. (2012), "The effect of near-fault directivity on building seismic collapse risk", *Earthq. Eng. Struct. Dyn.*, **41**(10), 1391-1409.
- Cheng, F.Y. and Pantelides, C.P. (1988), "Optimal placement of actuators for structural control", Technical Report No. NCEER-88-0037; National Center for Earthquake Engineering Research, State University of New York, Buffalo, NY, USA.

- Coley, D.A. (1999), An Introduction to Genetic Algorithms for Scientists and Engineers, World Scientific, Singapore.
- EC8 (2013), Design of Structures for Earthquake Resistance, Eurocode 8, European Committee for Standardization; Brussels, Belgium.
- FEMA P695 (2008), Quantification of Building Seismic Performance Factors, ATC-63 Project, Applied Technology Council, Redwood City, CA, USA.
- Gluck, N., Reinhorn, A.M., Gluck, J. and Levy, R. (1996), "Design of supplemental dampers for control of structures", *J. Struct. Eng.*, **122**(12), 1394-1399.
- Hoffman, E.W. and Richards, P.W. (2014), "Efficiently implementing genetic optimization with nonlinear response history analysis of taller buildings", *J. Struct. Eng.*, **140**(8), A4014011.
- Holland, J.H. (1992), *Adaptation in Natural and Artificial Systems*, MIT Press, Cambridge, MA, USA.
- Krawinkler, H. (1978), "Shear in beam-column joints in seismic design of frames", *Eng. J.*, **15**(2), 82-91.
- Lavan, O. and Levy, R. (2009), "Simple iterative use of Lyapunov's solution for the linear optimal seismic design of passive devices in framed buildings", *J. Earthq. Eng.*, **13**(5), 650-666.
- Levy, R. and Lavan, O. (2006), "Fully stressed design of passive controllers in framed structures for seismic loadings", *Struct. Multidisc. Optim.*, **32**(6), 485-498.
- Lignos, D.G. and Krawinkler, H. (2011), "Deterioration modeling of steel components in support of collapse prediction of steel moment frames under earthquake loading", *J. Struct. Eng.*, **137**(11), 1291-1302.
- Lignos, D.G., Krawinkler, H. and Whittaker, A.S. (2011), "Prediction and validation of sidesway collapse of two scale models of a 4-story steel moment frame", *Earthq. Eng. Struct. Dyn.*, **40**(7), 807-825.
- Lopez-Garcia, D. (2001), "A simple method for the design of optimal damper configurations in MDOF structures", *Earthq. Spectra*, **17**(3), 387-398.
- MATLAB (2014), Global Optimization Toolbox Release 2014b, The MathWorks, Natick, MA, USA.
- Miyamoto, H.K., Gilani, A.S.J., Wada, A. and Ariyaratana, C. (2010), "Limit states and failure mechanisms of viscous dampers and the implications for large earthquakes", *Earthq. Eng. Struct. Dyn.*, **39**(11), 1279-1297.
- Newell, J. and Uang, C.M. (2006), "Cyclic behavior of steel columns with combined high axial load and drift demand", Report No. SSRP-06/22, Department of Structural Engineering, University of California, San Diego, CA, USA.
- OpenSees (2016), Open System for Earthquake Engineering Simulation, Pacific Earthquake Engineering Research Center, University of California at Berkeley, Berkeley, CA, USA.
- Pacific Earthquake Engineering Research Center (PEER), NGA Database, <http://peer.berkeley.edu/nga>.
- Paola, M.D., Mendola, L.L. and Navarra, G. (2007), "Stochastic seismic analysis of structures with nonlinear viscous dampers", *J. Struct. Eng.*, **133**(10), 1475-1478.
- Ramirez, O.M., Constantinou, M.C., Gomez, J.D., Whittaker, A.S. and Chrysostomou, C.Z. (2002), "Evaluation of simplified methods of analysis of yielding structures with damping systems", *Earthq. Spectra*, **18**(3), 501-530.
- Ramirez, O.M., Constantinou, M.C., Whittaker, A.S., Kircher C.A. and Chrysostomou C.Z. (2002), "Elastic and inelastic seismic response of buildings with damping systems", *Earthq. Spectra*, **18**(3), 531-547.
- Seleemah, A.A. and Constantinou, M.C. (1997), "Investigation of seismic response of buildings with linear and nonlinear fluid viscous dampers", Technical Report No. NCEER-97-0004, National Center for Earthquake Engineering Research, State University of New York at Buffalo, Buffalo, NY, USA.
- Shukla, A.K. and Datta, T.K. (1999), "Optimal use of viscoelastic dampers in building frames for seismic response", *J. Struct. Eng.*, **125**(4), 401-409.
- Singh, M.P. and Moreshi, L.M. (2002), "Optimal placement of dampers for passive response control", *Earthq. Eng. Struct. Dyn.*, **31**(4), 955-976.
- Symans, M.D., Charney, F.A., Whittaker, A.S., Constantinou, M.C., Kircher, C.A., Johnson, M.W. and McNamara, R.J. (2008), "Energy dissipation systems for seismic applications: current practice and recent developments", *J. Struct. Eng.*, **134**(1), 3-21.
- Takewaki, I. (1997), "Optimal damper placement for minimum transfer functions", *Earthq. Eng. Struct. Dyn.*, **26**(11), 1113-1124.
- Takewaki, I. (2000), "Optimal damper placement for planar building frames using transfer functions", *Struct. Multidisc. Optim.*, **20**(4), 280-287.
- Taylor Devices Inc. (2017), <http://www.taylordevices.com>.
- Tzimas, A.S., Dimopoulos, A.I. and Karavasilis, T.L. (2015), "EC8-based seismic design and assessment of self-centering post-tensioned steel frames with viscous dampers", *J. Constr. Steel Res.*, **105**, 60-73.
- Vamvatsikos, D. and Cornell, C.A. (2002), "Incremental dynamic analysis", *Earthq. Eng. Struct. Dyn.*, **31**(3), 491-514.
- Whittle, J.K., Williams, M.S., Karavasilis, T.L. and Blakeborough, A. (2012), "A comparison of viscous damper placement methods for improving seismic building design", *J. Earthq. Eng.*, **16**(4), 540-560.
- Zhang, R.H. and Soong, T.T. (1992), "Seismic design of viscoelastic dampers for structural applications", *J. Struct. Eng.*, **118**(5), 1375-1392.

AT